



Contents lists available at ScienceDirect

Arabian Journal of Chemistry

journal homepage: www.ksu.edu.sa

Original article

Degradation of ribavirin by Fe²⁺/PS oxidation technology: performance, mechanism and toxicity controlXiaohui Sun^{a,b}, Wei Li^c, Zijun Dong^{a,b,*}, Yunhe Hou^c, Yuyang Ning^c, Chenyu Wang^{d,*}, Guo Lv^a^a College of Civil and Transportation Engineering, the Underground Polis Academy, Shenzhen University, Shenzhen 518060, China^b State Key Laboratory of Intelligent Geotechnics and Tunnelling (Shenzhen University), Shenzhen 518060, China^c Shenyang Jianzhu University, College of Municipal and Environmental Engineering, Shenyang 100168, China^d Jiangsu Collaborative Innovation Center of Atmospheric Environment and Equipment Technology (CICAET), Jiangsu Key Laboratory of Atmospheric Environment Monitoring and Pollution Control, School of Environmental Science and Engineering, Nanjing University of Information Science & Technology, Nanjing 210044, China

ARTICLE INFO

Keywords:

Ribavirin
Persulfate advanced oxidation
Ferrous activated
Mechanism

ABSTRACT

During the COVID-19 pandemic, the extensive use of ribavirin (RBV) raised concerns about its environmental residues and associated risks, necessitating remedial actions. This study investigates the degradation efficiency, mechanism, and biotoxicity of RBV using ferrous (Fe²⁺) activated persulfate (PS) advanced oxidation technology (Fe²⁺/PS oxidation). Experiments conducted under various conditions revealed that at pH = 3, PS concentration of 4 mM, PS/Fe²⁺ molar ratio of 2:1, and citric acid of 0.5 mM with Fe²⁺ added twice, the degradation rate of RBV reached 98.70 %. The degradation process of RBV by Fe²⁺/PS from 0 to 5 mins followed a first-order reaction kinetics model. The presence of halide ions (Cl⁻, Br⁻, I⁻) was found to inhibit the degradation efficiency. The active species involved were identified as SO₄^{-•}, ·OH, ¹O₂, and FeO²⁺, with SO₄^{-•} and ·OH being the most significant. Moreover, the products of ribavirin were determined and their degradation pathways were proposed. Dehydration, deamidation, C-N bond breaking and hydroxylation were the major pathways. Additionally, toxicity assessment showed that Fe²⁺/PS oxidation reduced the inhibition rate of bioluminescence in *Vibrio fischeri* from 31.58 % to 3.88 %, effectively controlling RBV toxicity during the reaction. This study provides insights into managing water environmental risks associated with pharmaceutical residues in the post-pandemic era.

1. Introduction

Ribavirin (RBV) has been widely listed as the potential antiviral drug to treat respiratory diseases since the COVID-2019 pandemic (Tarighi et al., 2021). In the post-pandemic era, an increasing amount of RBV and its metabolites are being released and consumed into the wastewater through human excretion, leaving potential environmental risks that continue to require attention. The reported concentrations of RBV in domestic wastewater, wastewater treatment plant (WWTP) effluent and rivers were as high as 2102, 207 and 52.2 ng/L, respectively (Guo et al., 2023). Its persistence and bioaccumulation posed a threat to natural ecosystems and human health. Karjadi et al. (2022) suggested that ribavirin had a significant inhibitory effect on the growth of crop roots. Ye et al. (2020) conducted in vitro bioassay using human induced pluripotent stem cells and conjectured that ribavirin might lead to DNA

damage and the accumulation of reactive oxygen species. However, RBV degradation by traditional biological treatment processes is very limited, only 2 % – 20 % removal rate being reported (Liu et al., 2022; Morales-Paredes et al., 2022). Therefore, it is necessary to introduce more efficient and green technologies to achieve RBV removal from water.

To address the above issues, many researches about advanced oxidation processes (AOPs) for RBV degradation have been developed and reported, such as photocatalysis, ozonation, electrocatalysis, Fenton, electrocoagulation etc (Dolatbadi et al., 2022; Tufail et al., 2021). These technologies mainly relied on the newly produced hydroxyl radical (·OH), which is non-selective to oxidize pollutants (Dolatbadi et al., 2023b; Jin et al., 2020). However, these technologies might have some drawbacks, such as high energy consumption, severe reaction conditions, excessive sludge production, secondary pollution risk, etc

* Corresponding authors.

E-mail addresses: dongzijun@szu.edu.cn (Z. Dong), wangchenyu@nuist.edu.cn (C. Wang).<https://doi.org/10.1016/j.arabjc.2024.105754>

Received 13 January 2024; Accepted 22 March 2024

Available online 26 March 2024

1878-5352/© 2024 The Authors. Published by Elsevier B.V. on behalf of King Saud University. This is an open access article under the CC BY-NC-ND license (<http://creativecommons.org/licenses/by-nc-nd/4.0/>).

(Dolatabadi et al., 2023a). In recent years, the persulfate advanced oxidation processes (PS-AOPs) have been as promising technologies in the field of wastewater treatment and groundwater pollution remediation, which was based on sulfate radical ($\text{SO}_4^{\cdot-}$) (Huang et al., 2021). Compared with other AOPs, the PS-AOPs have some distinctive advantages such as environmental friendliness, low cost, stability and simple operation (Wang et al., 2021; Yan et al., 2023). $\text{SO}_4^{\cdot-}$ has higher oxidation capacity ($E_0 = 2.7 - 3.1 \text{ V}$) than $\cdot\text{OH}$ ($E_0 = 1.9 - 2.7 \text{ V}$). In addition, $\text{SO}_4^{\cdot-}$ is more stable and cannot be easily disturbed by other background ions, thus having a wide range of applications.

Although PS is a very powerful oxidant, its reactions with pollutants are relatively slow. Thus, many researches have focused on activating PS through light, heat, transition metals and other means to generate active free radicals faster and more efficiently (Antoniu et al., 2010). Light-activated PS requires high water quality due to the light penetration ability involved. Thermal activation of PS makes thermal activation unsuitable for large-scale restoration due to the high demand for energy input (Wang and Wang, 2018). Metal-organic framework (MOF) activation of PS has an effective role, but cost is the biggest disadvantage (Su et al., 2023). Ferrous (Fe^{2+}) activated PS was simple with mild reaction conditions, no need of external energy consumption (such as heat and light source). Among of these methods, Fe^{2+} activated PS process gradually becomes to be one of wide applications. Thus, Fe^{2+} /PS oxidation technology has been used to oxidize and degrade many emerging contaminants (ECs) in water and soil, such as pyrene, triclosan, 2,4,6-trichloroanisole etc, with over 90 % removal rate being obtained (Chen et al., 2023; Gao et al., 2021; Zhang et al., 2018). However, most studies have put great emphasis on the removal efficiency of RBV itself. The evaluations of RBV degradation mechanism through the combination of laboratory instrument detection and quantum chemical theory calculation are still far less explored to date. In addition, the biotoxicity changes of the water samples during the reactions and controlling effect are large unknown.

Therefore, the objectives of this study were to systematically investigate the performance of Fe^{2+} /PS oxidation technology on RBV degradation, aiming to fill the gap in the application of this technology for RBV degradation, and to validate the feasibility of its application. Comprehensive studies on the degradation efficiency and mechanism of RBV in Fe^{2+} /PS oxidation were conducted through degradation experiments under various operational conditions, identification of active components, mass spectrometry analysis of products, and kinetic study. At last, the toxicity variation and controlling effect of the treated water samples were further evaluated.

2. Materials and methods

2.1. Chemicals and materials

RBV (purity $\geq 98 \%$, Sigma-Aldrich, USA) and PS (purity $\geq 97 \%$, Aladdin, China) were purchased and used without further purification. Other chemicals and reagents used in the experiments were of chromatographic of analytical pure. The solution used to prepare reagents in the test is ultrapure water (Milli-Q Direct 8, USA). Luminescent bacteria (the freeze-dried bacteria *Vibrio fischeri*) used for toxicity evaluation was purchased from SDIX Company in USA (DeltaTox) and stored at $-20 \text{ }^\circ\text{C}$.

2.2. Experimental methods

2.2.1. RBV degradation experiments

The degradation experiments of RBV were performed in 500 mL conical flasks. RBV solution with an initial concentration of 2.0 mg/L was prepared prior to the degradation reactions and added to the conical flask, following with the addition of hydrochloric acid or sodium hydroxide to adjust pH to the desired value. The reactions were initiated by

adding a certain quality of PS powder according to the experimental conditions. The reactions system was stirred at 350 r/min. 10 mL of treated samples were taken at different times and filtered through a 0.22 μm polyethersulfone membrane for further analysis. All the experiments were conducted at least twice.

2.2.2. Qualitative determination of active components

Some studies have confirmed that the active substances present in the Fe^{2+} /PS system are mostly $\text{SO}_4^{\cdot-}$ and $\cdot\text{OH}$; while some scholars have also proposed that FeO^{2+} is one of the active substances that sulfate being activated by ferrous (Wang et al., 2018). Therefore, in order to identify the active substances present in Fe^{2+} /PS oxidation system, this study has set up the electron paramagnetic resonance spectroscopy (EPR) tests, the free radical quenching tests, and FeO^{2+} capturing tests.

The EPR tests were applied for directly identifying the active components produced in Fe^{2+} /PS oxidation system. 5,5-Dimethyl-1-pyrroline N-oxide (DMPO) and 2,2,6,6-Tetramethylpiperidine (TEMP) were used to capture the active substances, such as $\text{SO}_4^{\cdot-}$, $\cdot\text{OH}$ and $^1\text{O}_2$, so as to form stable products DMPO- $\text{SO}_4^{\cdot-}$, DMPO- $\cdot\text{OH}$ and TEMP- $^1\text{O}_2$, which all with the specific signal peaks (Lian et al., 2019).

Methanol (MeOH) had a large reaction rate constant with $\text{SO}_4^{\cdot-}$ ($k_{\text{SO}_4^{\cdot-}, \text{MeOH}} = 1.1 \times 10^7 \text{ M}^{-1}\text{S}^{-1}$) and $\cdot\text{OH}$ ($k_{\cdot\text{OH}, \text{MeOH}} = 9.7 \times 10^8 \text{ M}^{-1}\text{S}^{-1}$), while tert butyl alcohol (TBA) had much larger reaction rate constant with $\cdot\text{OH}$ ($k_{\cdot\text{OH}, \text{TBA}} = 6.0 \times 10^8 \text{ M}^{-1}\text{S}^{-1}$) than that with $\text{SO}_4^{\cdot-}$ ($k_{\text{SO}_4^{\cdot-}, \text{TBA}} = 4.0 \times 10^5 \text{ M}^{-1}\text{S}^{-1}$) (Liu et al., 2021). Thus, MeOH was selected as the quencher of $\text{SO}_4^{\cdot-}$ and $\cdot\text{OH}$, while TBA as the quencher of $\cdot\text{OH}$. The concentrations of MeOH and TBA were both 2.0 M, which 10^5 times than that of RBV and could fully quench the produced free radicals during the reactions. The free radical quenching tests were carried out by adding a certain volume of MeOH and TBA in advance. The degradation rates of RBV were compared with the experiments without the quenching agents in order to assess the dominant species of free radicals.

2.2.3. Tracer experiment of sulfate radical and hydroxyl radical

The $\text{HO}\cdot$ can degrade nitrobenzene (NB) and atrazine (ATZ), whereas the $\text{SO}_4^{\cdot-}$ can only degrade ATZ. Therefore, by adding small amounts of NB and ATZ to the degradation system, the exposure values of $\text{SO}_4^{\cdot-}$ and $\text{HO}\cdot$ can be calculated based on the degradation rate and the second-order reaction constants with the active radicals. The specific formula for this calculation is as follows:

$$\left(\int [\text{HO}\cdot] dt \right)_{\text{NB}} = -\ln \left(\frac{[\text{NB}]_t}{[\text{NB}]_0} \right) / K_{(\text{HO}\cdot, \text{NB})} \quad (1)$$

$$\left(\int [\text{SO}_4^{\cdot-}] dt \right)_{\text{ATZ}} = \frac{-\ln \left(\frac{[\text{ATZ}]_t}{[\text{ATZ}]_0} \right) - K_{(\text{HO}\cdot, \text{ATZ})} \int [\text{HO}\cdot] dt}{K_{(\text{SO}_4^{\cdot-}, \text{ATZ})}} \quad (2)$$

where $K_{(\text{HO}\cdot, \text{NB})}$ and $K_{(\text{HO}\cdot, \text{ATZ})}$ represent the second-order reaction constant of $\text{HO}\cdot$ with NB and ATZ, respectively ($\text{M}^{-1}\cdot\text{S}^{-1}$). $K_{(\text{SO}_4^{\cdot-}, \text{NB})}$ is the second-order reaction constant of $\text{SO}_4^{\cdot-}$ with NB ($\text{M}^{-1}\cdot\text{S}^{-1}$), $(\int [\text{HO}\cdot] dt)_{\text{NB}}$ and $(\int [\text{SO}_4^{\cdot-}] dt)_{\text{NB}}$ refer to the exposure value of $\text{HO}\cdot$ ($\text{M}\cdot\text{S}$) obtained using NB and ATT as a tracer, respectively.

In Fe^{2+} /PS oxidation system, there also existed the non-free radical active component FeO^{2+} , which could react with tetramethylene sulfide (TMSO) to form tetramethylsulfoxide (TMSO_2). Thus, the FeO^{2+} capturing tests were carried out by adding 0.5 mM TMSO before the start of RBV degradation and detecting the content of TMSO_2 to calculate the concentration of FeO^{2+} . The quantification of TMSO and TMSO_2 is achieved through High-performance liquid chromatography (HPLC). Chromatographic conditions include operating at $35 \text{ }^\circ\text{C}$ using a C18 column ($4.6 \times 150 \text{ mm}$, $5 \mu\text{m}$), with an isocratic elution of acetonitrile/water (60/40 v/v) at a flow rate of 1 mL/min. The injection volume is set at 100 μL , and ultraviolet detection is conducted at a wavelength of 212 nm.

2.3. Analytical methods

The concentration of RBV was determined by using a HPLC (7980, Waters, USA), equipped with a UV-vis detector and a C18 column (4.6 mm × 150 mm, 5 μm) at 35 °C. The mobile phase consisted of methanol/water (20 / 80) at a flow rate of 1 mL/min. The injection volume was 100 μL, and the detection wavelength was 209 nm.

The presence of Fe⁴⁺ (FeO²⁺) was determined by adding TMSO to the experimental system. TMSO and TMSO₂ were detected by HPLC under the following chromatographic conditions: C18 column (4.6 × 150 mm, 5 μm), column temperature 35 °C, mobile phase acetonitrile/water (60 / 40), injection volume 100 μL, isocratic elution with flow rate at 1 mL/min, UV detection wavelength 212 nm.

The degradation products (DPs) of RBV were analyzed using a LC-MS system (1290-AB SICEX Triple, Agilent, USA). The specific testing methods were detailed in the “Supplementary Material (Text S1)”. The solution pH was detected by a portable digital pH meter (pHS-3B, Shanghai Hongyi, China).

The comprehensive biological toxicity of the water samples during RBV degradation was evaluated by TX1315 toxicity detection analyzer (TX1315, HACH, USA), which was according to the ISO standard luminescent bacteria toxicity test. The specific steps were as followed in the “Supplementary Material (Text S2)”. The results of the toxicity test were characterized by the relative inhibitory rate (T%) of luminescent bacteria, which was calculated with the formula shown below.

$$T\% = \frac{E_0 - E}{E_0} \times 100\% \quad (3)$$

where E_0 and E represents initial and measured luminescence, respectively.

3. Results and discussion

3.1. The degradation performance of RBV in different system

To determine the degradation capability of the Fe²⁺/PS system on RBV, four experimental groups were set up: PS alone, Fe²⁺ alone, simultaneous addition of both, and a control group. Other conditions included a pH of 3, room temperature, and a reaction time of 60 min. Post-reaction sampling and RBV concentration measurement revealed the degradation performance as shown in Fig. 1.

It was observed that the group with only Fe²⁺ added showed

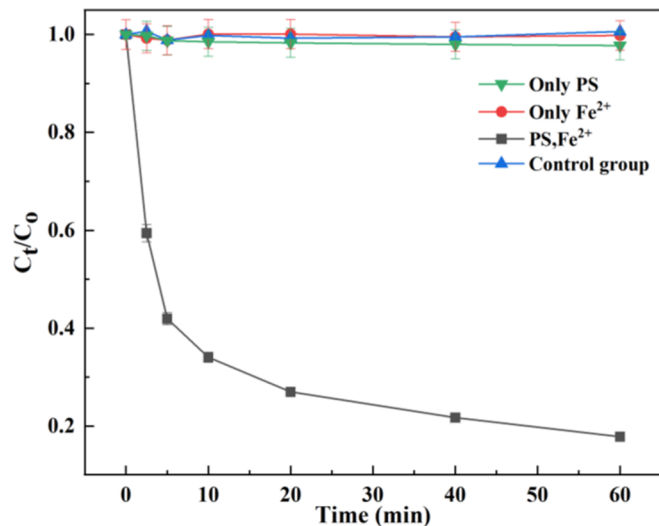


Fig. 1. Degradation of ribavirin by adding PS, Fe²⁺ alone, adding both at the same time or not adding either (control group). [RBV]₀ = 2.0 mg/L, [PS]₀ = 4.00 mM, [Fe²⁺]₀ = 2.00 mM, [pH]₀ = 3, t = 60 min.

negligible degradation of RBV after 60 min, similar to the control group, indicating that Fe²⁺ alone does not degrade RBV. A slight reduction in RBV was noted with PS alone. However, in the Fe²⁺/PS system, the RBV concentration significantly decreased, with a degradation rate of 82.17 % after 60 min. Although PS is a strong oxidant, it reacts slowly with organic substances and requires activation to generate reactive radicals that enhance pollutant degradation. This explains why the degradation effect of RBV in the combined PS and Fe²⁺ experiment was significantly better than in the first three experiments. Fe²⁺ activates PS to produce reactive radicals, thereby removing RBV. These results demonstrate the evident degradation capability of the Fe²⁺/PS system on RBV. Compared with other AOPs processes, Fe²⁺/PS also demonstrates certain advantages in degradation performance. For instance, Wu et al. (2022) utilized UV/TiO₂/H₂O₂ process, achieving an approximate 80 % degradation rate of RBV with a H₂O₂ dosage of 0.5 ‰; Liu et al. (2021) employed PMS/O₃ process, yielding less than 50 % degradation rate of RBV (PMS = 0.025 mM, O₃ = 0.025 mM). The degradation rates reported in these studies are lower than that of RBV degradation by Fe²⁺/PS in our research. Reaction stoichiometric efficiency is a crucial parameter to evaluate the catalyst performance. The catalytic performance of PS by Fe²⁺ in Fe²⁺/PS was calculated by the method in Text S3 and %RSE was obtained as 0.424 %. We summarize the %RSE in the different PS systems (Table S1) and find that Fe²⁺/PS is lower than the other systems. Future studies should focus on optimizing the reaction conditions to improve %RSE for avoiding any loss of energy and materials.

3.2. The degradation mechanism of RBV

3.2.1. Identification of active components during RBV degradation

To directly confirm the presence of ·OH and SO₄· radicals during the oxidation of RBV in the Fe²⁺/PS system, EPR spectroscopy was employed. DMPO was used to capture free radicals, with the EPR spectra scanned using an electron spin resonance spectrometer. The EPR spectra, as shown in Fig. 2(a), revealed the detection of four DMPO-OH characteristic peaks (intensity ratio 1:2:2:1) and six DMPO-SO₄ peaks in the Fe²⁺/PS added experimental group. This confirmed the existence of ·OH and SO₄· during the RBV oxidation process in the Fe²⁺/PS system. The high degradation rate of RBV by Fe²⁺/PS oxidation further substantiates the role of ·OH and SO₄· in the system's degradation mechanism of RBV.

Additionally, the spectra revealed that in samples where only PS was added, neither DMPO-OH nor DMPO-SO₄ peaks were detected. However, a minor degradation of RBV was still observed in these PS-only experiments, suggesting the presence of active species other than ·OH and SO₄· in the Fe²⁺/PS system. EPR spectroscopy using TEMP as a radical trap was thus employed to detect these species. The EPR spectra, as shown in Fig. 2(b), indicated the presence of three characteristic TEMP-¹O₂ peaks with an intensity ratio of 1:1:1 in both PS-only and Fe²⁺/PS-added samples, signifying ¹O₂ as another active species involved in RBV oxidation. Notably, the intensity of TEMP-¹O₂ peaks in the Fe²⁺/PS group was significantly higher than in the PS-only group, indicating enhanced ¹O₂ generation upon the addition of Fe²⁺. ·OH and other reaction intermediates may ultimately be converted into ¹O₂ through a series of complex reaction pathways. Considering that no DMPO-OH was detected in the sample with only PS added, so the main source of ¹O₂ in the PS system may be the conversion of other intermediate products. Existing studies suggest that ¹O₂ can selectively oxidize and degrade recalcitrant pollutants in water, though its activity in degrading saturated alcohols like ethanol, methanol, and *tert*-butanol is negligible (Hong et al., 2021).

FeO²⁺ is another non-radical active component in the Fe²⁺/PS system (Zhou et al., 2023). Experiments under optimal conditions were initiated with the addition of 0.5 mM TMSO. Sampling at different intervals to detect TMSO₂ concentrations allowed for estimation of FeO²⁺ concentration changes, as illustrated in Fig. 2(c). The generation of

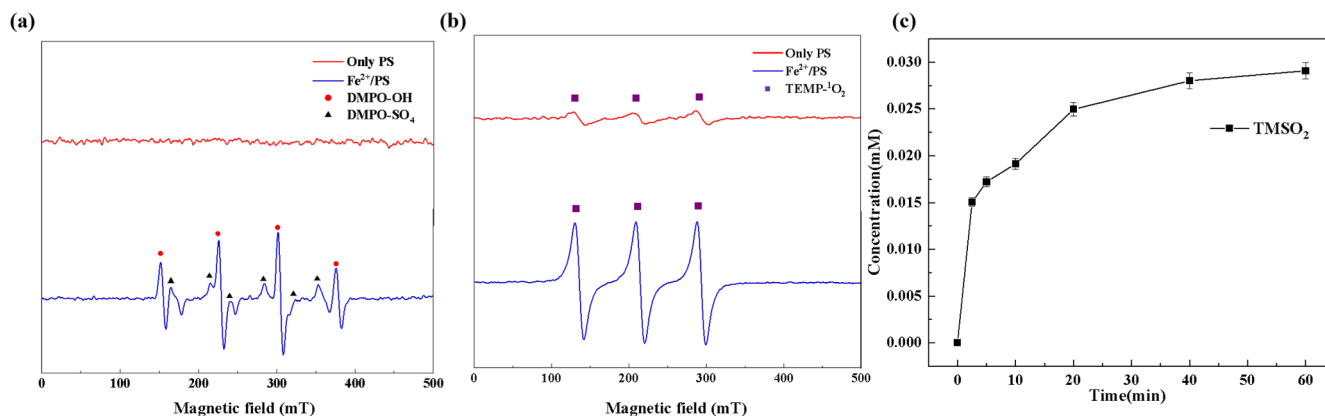


Fig. 2. EPR spectra of (a) DMPO-OH and DMPO-SO₄, (b) TEMP-¹O₂ in RBV Fe²⁺/PS oxidation process and (c) TMSO₂ concentration for FeO₂⁺ measure, for FeO₂⁺ measure test, the [RBV]₀ = 2.0 mg/L, initial pH = 3, [PS]₀ = 4.0 mM, [PS/Fe²⁺] = 2/1, [CA]₀ = 0.5 mM, add in Fe²⁺ in twice, [TMSO]₀ = 0.5 mM).

TMSO₂ indicates the presence of FeO₂⁺ in the Fe²⁺/PS system. However, the sulfonation rate of approximately 6.00 % indirectly suggests a minor contribution of FeO₂⁺ to RBV degradation. This could be attributed to the instability of FeO₂⁺ under acidic conditions, as previous study indicates a higher stability of FeO₂⁺ in alkaline conditions, providing sufficient time for interaction with pollutants (Koppenol, 2022).

3.2.2. Contribution of active components in RBV degradation

Alcohol inhibition experiments were conducted to study the contributions of ·OH and SO₄^{·-} to the degradation of RBV. The impact of various alcohols on RBV degradation is depicted in Fig. 3(a). It was observed that MeOH and TBA significantly inhibited RBV degradation, with MeOH exhibiting a higher inhibition rate than TBA. The degradation rates of RBV in the absence of alcohol, with MeOH, and with TBA were 96.01 %, 11.14 %, and 66.27 %, respectively, indicating the predominant contribution of SO₄^{·-}, followed by ·OH. The addition of MeOH did not inhibit the action of ¹O₂ due to its low reaction rate with ¹O₂, suggesting that ¹O₂ does not play a major role in RBV degradation.

Radical tracer experiments, as shown in Fig. 3(b), further indirectly confirm that ·OH and SO₄^{·-} are the active components in the Fe²⁺/PS oxidation process of RBV, with the exposure value of SO₄^{·-} being significantly higher than that of ·OH, indicating a stronger degradation effect of SO₄^{·-} on RBV. At 10 mins into the reaction, there was a substantial

increase in the exposure values of the radicals, due to the activation of PS by the second addition of Fe²⁺, generating a large amount of ·OH and SO₄^{·-}.

3.2.3. RBV degradation products and pathways

Using HPLC-MS, ten products with *m/z* values of 113, 147, 198, 211, 241, 256, 283, 338, 340, and 344 were detected. Liu et al. (2021) identified five DPs of RBV with *m/z* values of 241, 211, 198, and 147. Thus, four identifiable DPs were determined as DP-1, DP-2, DP-3, and DP-4, with corresponding mass spectral parameters listed in Table 1. DP-1, with an *m/z* of 241, slightly lower than RBV's 245, indicates the presence of alcohol, carbonyl, and amide groups in RBV. The increased unsaturation suggests DP-1 as a hydroxyl dehydrogenation product. Researchers have demonstrated through quantum chemical calculations that the amide group is likely susceptible to attack (Liu et al., 2021). DP-2 and DP-3, based on their mass difference from DP-1, are hypothesized to be the de-alcoholized and de-amidized degradation products of DP-1, respectively. DP-3 may undergo C-N bond breakage and hydroxylation, transforming into DP-4. Therefore, a possible RBV degradation pathway, based on the above analysis, is proposed in Fig. 4. The mineralization of RBV in the system was determined to be 13.1 % by total organic carbon (TOC) analyzer (Fig. S5). Combined with the fact that the detected products of RBV are macromolecules it can be seen that the degradation

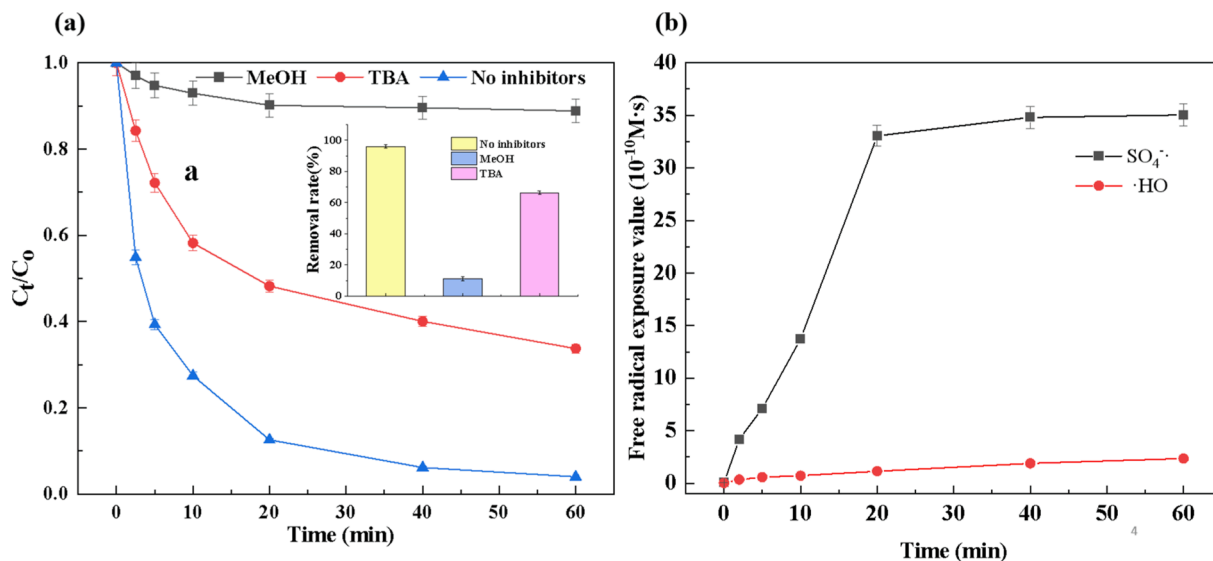


Fig. 3. (a) Effect of different alcohols on the degradation rate of RBV ([RBV]₀ = 2.0 mg/L, initial pH = 3, [PS]₀ = 4.0 mM, [PS/Fe²⁺] = 2/1, [CA]₀ = 0.5 mM, add in Fe²⁺ in twice, [MeOH] = 2.0 M, [TBA] = 2.0 M), (b) Radical tracer experiments of SO₄^{·-} and OH·.

Table 1
Mass spectrometry parameters of the four degradation products.

	Retention time	Molecular formula	Relative molecular mass	ESI(+)/MS (<i>m/z</i>)	Structural
DP-1	7.45 min	C ₈ H ₈ N ₄ O ₅	240	241	
DP-2	6.22 min	C ₇ H ₆ N ₄ O ₄	210	211	
DP-3	5.92 min	C ₇ H ₇ N ₃ O ₄	197	198	
DP-4	8.20 min	C ₅ H ₆ O ₅	146	147	

of RBV by the PS/Fe²⁺ system is not sufficient.

3.3. The effect factors of Fe²⁺/PS oxidation system on RBV degradation

To enhance the degradation efficiency of the Fe²⁺/PS oxidation system for RBV, the influence of operational conditions on RBV degradation was further investigated.

3.3.1. Impact of initial pH on RBV degradation

The effects of different initial pH levels on RBV degradation are presented in Fig. 5. Results indicate that acidic conditions generally promote higher degradation rates compared to neutral and alkaline conditions. At pH 9, the degradation rate drops to its lowest at 24.22 %. However, the optimal initial pH for RBV degradation is identified as 3, achieving a degradation rate of 82.18 %. The enhanced efficiency under acidic conditions is attributed to multiple factors: (1) Formation of Fe²⁺ complexes at pH > 4.0 impedes the reaction between Fe²⁺ and PS, leading to Fe²⁺ precipitation as Fe³⁺ ions, reducing the available Fe²⁺ and consequently diminishing PS activation (Xu and Li, 2010); (2) SO₄^{•-} exhibits higher redox potential in acidic solutions, resulting in higher degradation rates (Romero et al., 2010). At pH 2, the degradation rate of RBV is 54.57 %, lower than at pH 3, possibly due to reduced radical quantities at lower pH levels, as corroborated by Khan and Adewuyi, (2010).

3.3.2. Impact of reagents on RBV degradation

The influence of varying PS concentrations on RBV degradation is illustrated in Fig. 6(a). An initial increase in degradation rate is observed with rising PS molar concentrations, peaking when the concentration

shifts from 2 mM to 4 mM, elevating RBV degradation from 71.70 % to 83.88 %. This enhancement is attributed to an increase in active radicals generated upon PS activation. However, degradation stabilizes with further PS concentration increments, as demonstrated at 6 mM and 8 mM, yielding RBV removal rates of 81.39 % and 80.69 %, respectively. This indicates that at 4 mM PS, sufficient active radicals for RBV

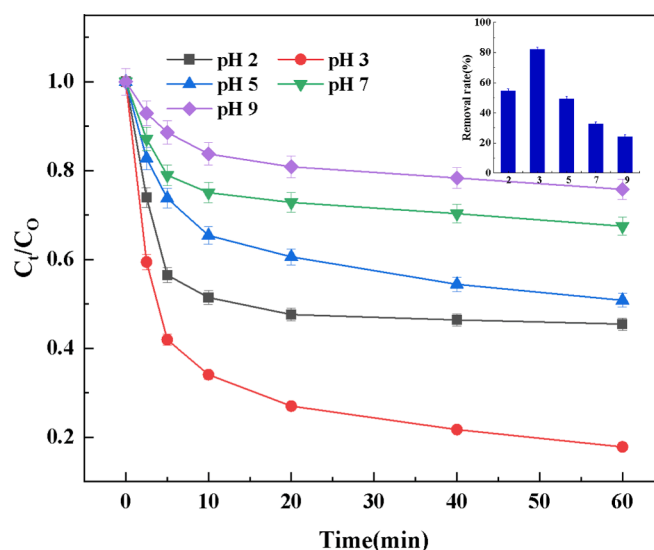


Fig. 5. Effect of different initial pH on the degradation of RBV. Initial experimental conditions: [RBV]₀ = 8.0 μM, [PS]₀ = 4.0 mM, [Fe²⁺]₀ = 2.0 mM.

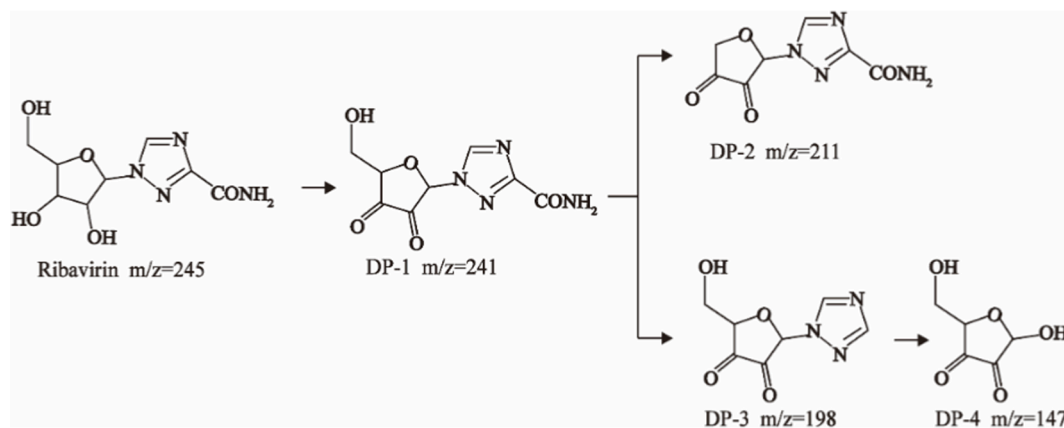


Fig. 4. Possible RBV degradation pathway.

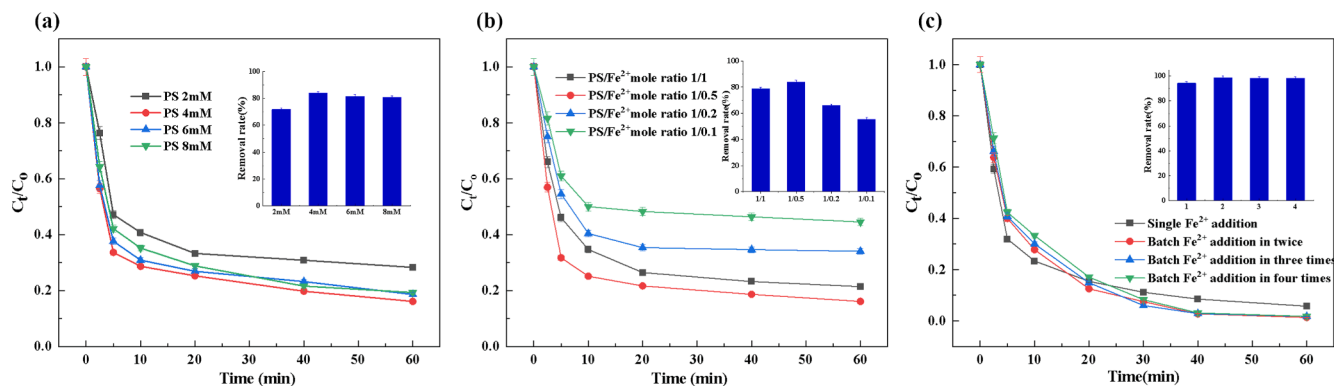


Fig. 6. Effects of (a) different PS concentrations ($[RBV]_0 = 2.0$ mg/L, initial pH = 3, $[Fe^{2+}]_0 = 2.0$ mM), (b) different PS/ Fe^{2+} molar ratio ($[RBV]_0 = 2.0$ mg/L, initial pH = 3, $[PS]_0 = 4.0$ mM) and (c) different Fe^{2+} dosage on the degradation of RBV ($[RBV]_0 = 2.0$ mg/L, initial pH = 3, $[PS]_0 = 4.0$ mM, $[PS/Fe^{2+}] = 2/1$, $[CA]_0 = 0.5$ mM) on the degradation of RBV.

degradation are produced under the experimental conditions of this study.

Additionally, altering PS/ Fe^{2+} molar ratios under a 4 mM PS concentration was explored for its effect on RBV degradation, as shown in Fig. 6(b). RBV removal rates initially increase then decrease with rising Fe^{2+} concentrations. A PS/ Fe^{2+} molar ratio of 1/0.1 results in a 55.47% degradation rate at reaction completion. Increasing Fe^{2+} to a 1/0.5 PS/ Fe^{2+} ratio enhances the degradation rate to 83.86%. However, further Fe^{2+} increments hinder RBV degradation, with a 1/1 PS/ Fe^{2+} ratio resulting in only a 78.59% degradation rate. Similar findings by Chen et al. (2009) suggest that organic matter degradation initially increases and then decreases with rising Fe^{2+} concentrations. They explain that an increase in Fe^{2+} enhances $SO_4^{\cdot-}$ generation from PS activation (Eq. (4)), thus elevating RBV degradation rates. Conversely, excess Fe^{2+} competes for $SO_4^{\cdot-}$, forming sulfate (Eq. (5)), thereby diminishing RBV degradation capacity. Consequently, a PS/ Fe^{2+} molar ratio of 1/0.5 is identified as the optimal ratio for RBV degradation in the Fe^{2+} /PS system.



The impact of different Fe^{2+} addition methods on RBV degradation was additionally investigated, as shown in Fig. 6(c). In the Fe^{2+} /PS system, a single addition of Fe^{2+} resulted in a lower RBV degradation rate compared to batch additions. The RBV removal rate with a single

Fe^{2+} addition was 94.27%, whereas batch additions of Fe^{2+} consistently achieved degradation rates over 98.00%. The highest removal rate, reaching 98.70%, was observed with two separate additions of Fe^{2+} . Shang et al. (2019) also discovered that batch addition of Fe^{2+} increased the removal rate of diatrizoate by 61%. This phenomenon can be attributed to the gradual, batch addition of Fe^{2+} , leading to a slower generation of $SO_4^{\cdot-}$ in the system, which allows for more effective interaction between RBV and the radicals, thereby enhancing the degradation rate.

3.3.3. Influence of reaction environment on RBV degradation

In addition to initial pH and reagent addition, other coexisting components in the reaction environment can also impact the degradation of RBV by the Fe^{2+} /PS oxidation system. Citric acid (CA), a green chelating agent, has been confirmed by Han et al. (2015) to significantly enhance the activation of Fe^{2+} on PS. Consequently, this study explored the impact of different concentrations of CA on RBV degradation in the Fe^{2+} /PS system, as shown in Fig. 7(a). When the CA concentration increased from 0 mM to 0.5 mM, the removal rate of RBV rose from 83.02% to 95.53%. However, further increases in CA concentration led to a decrease in RBV removal. At a CA concentration of 2 mM, the RBV removal rate was 87.27%. Zeng et al. (2021) reached similar conclusions in his study on the degradation of naphthalene solutions using Fe^{2+} activated persulfate coupled with CA, attributing the effect to CA preventing Fe^{2+} precipitation and promoting the generation of active

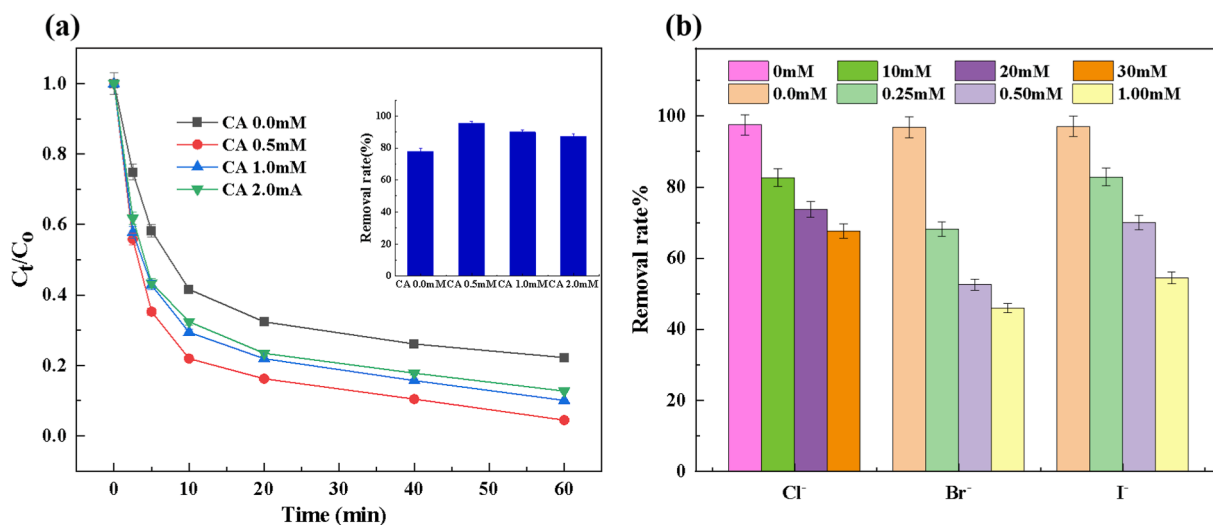


Fig. 7. Effects of (a) different molar ratios of citric acid (CA) ($[RBV]_0 = 2.0$ mg/L, initial pH = 3, $[PS]_0 = 4.0$ mM, $[PS/Fe^{2+}] = 2/1$) and (b) different halogen ion concentrations on the degradation of RBV ($[RBV]_0 = 2.0$ mg/L, initial pH = 3, $[PS]_0 = 4.0$ mM, $[PS/Fe^{2+}] = 2/1$, $[CA]_0 = 0.5$ mM, add in Fe^{2+} in twice).

Table 2
Kinetic fitting of RBV degradation.

Test Group		K_{obs}^a (min ⁻¹) in 0–5 min	R ² for 0–5 min	R ² for all data
Initial pH	2	0.1156	0.999	0.491
	3	0.1806	0.985	0.733
	5	0.0638	0.977	0.758
	7	0.0488	0.989	0.625
	9	0.0252	0.982	0.746
PS concentration	2	0.1419	0.969	0.624
	4	0.2200	0.999	0.666
	6	0.2004	0.994	0.653
	8	0.1736	0.999	0.726
PS/Fe ²⁺ molar ratio	1/1	0.1573	0.998	0.675
	1/0.5	0.2288	0.999	0.597
	1/0.2	0.1199	0.999	0.553
	1/0.1	0.0954	0.988	0.543

^a Apparent kinetic rate constant.

radicals. Excessive CA forms highly stable chelates with Fe²⁺, which is not conducive to catalytic reaction of Fe²⁺ (Rastogi et al., 2009). Huang et al. (2005) also mentioned in his research that high concentrations of citrate compete with target pollutants for SO₄^{•-}.

Halide ions, commonly found in natural water bodies, were detected in a river in Shenzhen, China, with concentrations of Cl⁻, Br⁻, and I⁻, where Cl⁻ reached up to 3200 mg/L (Shi et al., 2018). Yang et al. (2014) noted that halides compete with pollutants for reactive species, making it essential to understand their influence on RBV degradation in the Fe²⁺/PS system. The effect of varying concentrations of halide ions on RBV degradation in the Fe²⁺/PS process is shown in Fig. 7(b). All three halides inhibited RBV degradation, with the effect intensifying at higher ion concentrations. This correlates with halide reactions forming weaker halogen radicals compared to ·OH and SO₄^{•-}, as indicated in Eqs. (6) – (10) (Zhang and Parker, 2018). For instance, Cl⁻ and Cl₂⁻ have lower oxidation potentials than SO₄^{•-} and ·OH. Thus, the presence of halide ions reduces the Fe²⁺/PS removal rate of RBV. A first-order kinetics fit was conducted to understand the rate changes under different conditions.



3.3.4. RBV degradation kinetics

Pseudo first-order kinetic fitting was applied to RBV degradation under various operational conditions (Table 2) as Eq. (11).

$$\ln(C_t/C_0) = -k_{obs}t \quad (11)$$

where C_t and C_0 is RBV concentration at reaction time t and initial concentration, respectively. The k_{obs} is apparent kinetic rate constant, t refers to reaction time.

It was found that during the initial 5 min, the degradation process followed a first-order kinetic model, with fitting R² values above 0.969. However, as the reaction progressed, the process no longer followed this model, with R² values dropping to 0.491 – 0.758 when fitting 0 – 60 min data. In the subsequent degradation process, the degradation rate decreases, resulting in no longer following the first-order reaction kinetics. This could be attributed to the rapid consumption of radicals due to RBV degradation, resulting in a deviation from first-order kinetics as reactant concentrations decreased. The result indicates the relatively rapid degradation efficiency of RBV by PS/Fe²⁺. Besides, it also suggests that achieving complete degradation of RBV requires a more sufficient dosage of reagents.

Experiments on factors affecting the degradation efficiency in the Fe²⁺/PS system indicated that optimal RBV degradation was achieved at pH = 3, [PS] = 4 mM, and a PS/Fe²⁺ molar ratio of 1/0.5. Kinetic study demonstrated a correlation between apparent kinetic constants and reaction conditions, with the highest constants observed under optimal degradation conditions.

3.4. Biototoxicity assessment of DPs

During the degradation of pollutants, more toxic byproducts may be formed. Therefore, to determine the least toxic reaction time in the RBV degradation process, a sequential biototoxicity test was performed. The inhibition rate of bioluminescence in *Vibrio fischeri* at different reaction times is shown in Fig. 8. A general declining trend in toxicity was observed, indicating a reduction in system toxicity over time. The most significant decrease occurred within the first 30 min, with the inhibition rate dropping from 31.58 % to 15.98 %, likely due to the rapid degradation of RBV by abundant reactive species formed at the start of the reaction. Between 30 and 60 min, the inhibition rate first increased, then decreased, and increased again, with rates at 40, 50, and 60 min being 16.67 %, 11.91 %, and 13.23 % respectively. This fluctuation might be due to the formation of more toxic byproducts during these periods, as also indicated in studies by An et al. (2015a) and An et al. (2015b). Continuing the reaction up to 150 min led to a further decrease in

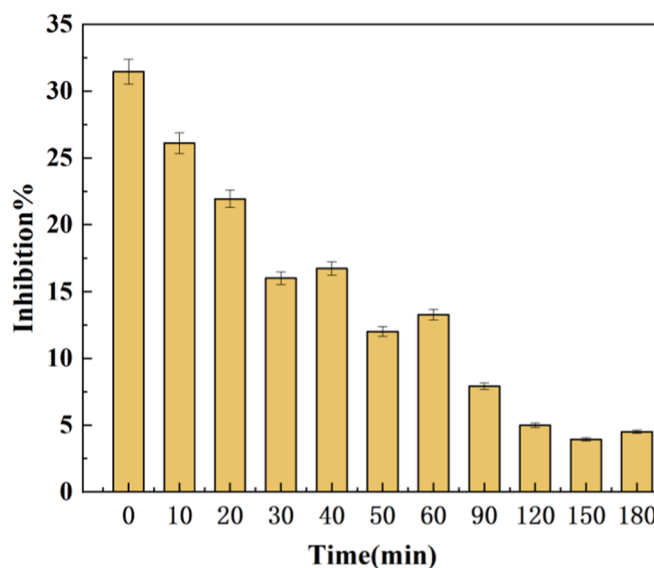


Fig. 8. Inhibition rate of luminescent of *Vibrio fischeri* from RBV degraded by Fe²⁺/PS at different time ([RBV]₀ = 2.0 mg/L, [pH]₀ = 3, [PS]₀ = 4.0 mM, [PS/Fe²⁺] = 2/1, [CA]₀ = 0.5 mM, add in Fe²⁺ in twice).

toxicity to 3.88 %. However, a slight increase in toxicity was observed between 150 and 180 min, possibly due to the formation of toxic degradation products. Therefore, based on these results, the optimal degradation time for RBV should be controlled between 120 and 150 min to avoid the formation of toxic byproducts. However, it should be noted that this is only the preliminary conclusions based on the current single batch experiment, and further detailed exploration is still needed in conjunction with the corresponding toxicology model study.

4. Conclusion

This study systematically investigated the degradation of RBV by the Fe^{2+} /PS system, demonstrating its significant effectiveness. Optimal degradation (98.70 %) was achieved at pH = 3, PS concentration of 4 mM, PS/ Fe^{2+} molar ratio of 2:1, and CA concentration of 0.5 mM, with two additions of Fe^{2+} . The impact of coexisting components in the reaction environment on the degradation of RBV were also discussed, such as CA and halide ions. The process followed first-order kinetics within the initial 0–5 min, while due to the rapid consumption of radicals with RBV degradation, resulting in a deviation from first-order kinetics as reactant concentrations decreased. Furthermore, compared to existing studies that focuses more on degradation efficiency, the degradation mechanisms and biotoxicity assessment were also investigated. Active species such as SO_4^- , $\cdot\text{OH}$, $^1\text{O}_2$, and FeO^{2+} were identified, with SO_4^- and $\cdot\text{OH}$ playing major roles. Four organic RBV degradation products were detected, proposing a degradation mechanism based on active species and product characterization. Toxicity assessment showed a reduction in *Vibrio fischeri* inhibition rate from 31.58 % to 3.88 %. This research provides a reference for addressing water environmental risks of pharmaceutical residues post-pandemic, and fill the gap in the application of Fe^{2+} /PS technology for RBV degradation. Further studies are required to validate degradation efficiency in real-world scenarios and consider the influence of coexisting natural water conditions on the degradation process.

CRedit authorship contribution statement

Xiaohui Sun: Conceptualization, Data curation, Formal analysis, Funding acquisition, Writing – review & editing. **Wei Li:** Investigation, Resources, Software, Supervision, Validation, Visualization. **Zijun Dong:** Conceptualization, Funding acquisition, Investigation, Resources, Software, Supervision, Validation, Visualization, Writing – original draft, Writing – review & editing. **Yunhe Hou:** Project administration, Resources, Software, Validation. **Yuyang Ning:** Writing – review & editing. **Chenyu Wang:** Software, Supervision, Validation, Visualization, Writing – original draft, Writing – review & editing. **Guo Lv:** Methodology, Project administration.

Declaration of competing interest

The authors declare that they have no known competing financial interests or personal relationships that could have appeared to influence the work reported in this paper.

Acknowledgement

This research was supported by the funds of National Natural Science Foundation of China (42277373, 52170007), Shenzhen Sustainable Development Project (KCXFZ20201221173413037, KCXFZ20211020164013020).

Appendix A. Supplementary data

Supplementary data to this article can be found online at <https://doi.org/10.1016/j.arabjc.2024.105754>.

References

- An, T., An, J., Gao, Y., Li, G., Fang, H., Song, W., 2015b. Photocatalytic degradation and mineralization mechanism and toxicity assessment of antiviral drug acyclovir: experimental and theoretical studies. *Appl. Catal. B* 164, 279–287. <https://doi.org/10.1016/j.apcatb.2014.09.009>.
- An, J., Li, G., An, T., Song, W., Feng, H., Lu, Y., 2015a. Photocatalytic degradation of three amantadine antiviral drugs as well as their eco-toxicity evolution. *Catal. Today*, Selected contributions in the field of heterogeneous catalysis and photocatalysis that were presented at the 8th Int. Conference on Environ. Catal. (ICEC 2014) 258, 602–609. <https://doi.org/10.1016/j.cattod.2015.01.004>.
- Antoniou, M.G., de la Cruz, A.A., Dionysiou, D.D., 2010. Degradation of microcystin-LR using sulfate radicals generated through photolysis, thermolysis and e⁻ transfer mechanisms. *Appl. Catal. B* 96, 290–298. <https://doi.org/10.1016/j.apcatb.2010.02.013>.
- Chen, L., Dong, X., Feng, R., Li, W., Ding, D., Cai, T., Jiang, C., 2023. Oxalic acid enhanced ferrous/persulfate process for the degradation of triclosan in soil: efficiency, mechanism and a column study. *Chem. Eng. J.* 473, 144961 <https://doi.org/10.1016/j.cej.2023.144961>.
- Chen, K.F., Kao, C.M., Wu, L.C., Surampalli, R.Y., Liang, S.H., 2009. Methyl tert-butyl ether (MTBE) degradation by ferrous ion-activated persulfate oxidation: feasibility and kinetics studies. *Water Environ. Res.* 81, 687–694. <https://doi.org/10.2175/106143008X370539>.
- Dolatabadi, M., Kheirieh, A., Yoosefian, M., Ahmadzadeh, S., 2022. Hydroxylamine removal from the polluted aqueous solution using the hybrid treatment process of electrocoagulation and adsorption; optimization, and modeling. *Appl. Water Sci.* 12, 254. <https://doi.org/10.1007/s13201-022-01780-7>.
- Dolatabadi, M., Ehrampoush, M.H., Pourmandari, M., Ebrahimi, A.A., Fallahzadeh, H., Ahmadzadeh, S., 2023a. Enhanced electrocatalytic elimination of fenitrothion, trifluralin, and chlorothalonil from groundwater and industrial wastewater using modified Cu-PbO₂ electrode. *J. Mol. Liq.* 379, 121706 <https://doi.org/10.1016/j.molliq.2023.121706>.
- Dolatabadi, M., Świergosz, T., Wang, C., Ahmadzadeh, S., 2023b. Accelerated degradation of groundwater-containing malathion using persulfate activated magnetic Fe₃O₄/graphene oxide nanocomposite for advanced water treatment. *Arab. J. Chem.* 16, 104424 <https://doi.org/10.1016/j.arabjc.2022.104424>.
- Gao, Y., Yang, F., Jian, H., Zhen, K., Zhang, P., Tang, X., Fu, Z., Xu, W., Wang, C., Sun, H., 2021. Pyrene degradation in an aqueous system using ferrous citrate complex activated persulfate over a wide pH range. *J. Environ. Chem. Eng.* 9, 106733 <https://doi.org/10.1016/j.jece.2021.106733>.
- Guo, Z., He, H., Liu, K., Li, Z., Yang, S., Liao, Z., Lai, C., Ren, X., Huang, B., Pan, X., 2023. The photolytic behavior of COVID-19 antivirals ribavirin in natural waters and the increased environmental risk. *J. Hazard. Mater.* 452, 131320 <https://doi.org/10.1016/j.jhazmat.2023.131320>.
- Han, D., Wan, J., Ma, Y., Wang, Y., Li, Y., Li, D., Guan, Z., 2015. New insights into the role of organic chelating agents in Fe(II) activated persulfate processes. *Chem. Eng. J.* 269, 425–433. <https://doi.org/10.1016/j.cej.2015.01.106>.
- Hong, P., Wu, Z., Yang, D., Zhang, K., He, J., Li, Y., Xie, C., Yang, W., Yang, Y., Kong, L., Liu, J., 2021. Efficient generation of singlet oxygen (1O₂) by hollow amorphous Co/C composites for selective degradation of oxytetracycline via fenton-like process. *Chem. Eng. J.* 421, 129594 <https://doi.org/10.1016/j.cej.2021.129594>.
- Huang, W., Xiao, S., Zhong, H., Yan, M., Yang, X., 2021. Activation of persulfates by carbonaceous materials: a review. *Chem. Eng. J.* 418, 129297 <https://doi.org/10.1016/j.cej.2021.129297>.
- Huang, K.-C., Zhao, Z., Hoag, G.E., Dahmani, A., Block, P.A., 2005. Degradation of volatile organic compounds with thermally activated persulfate oxidation. *Chemosphere* 61, 551–560. <https://doi.org/10.1016/j.chemosphere.2005.02.032>.
- Jin, X., Wu, Y., Zhang, Q., Wang, F., Chen, P., Liu, H., Huang, S., Wu, J., Tu, N., Lv, W., Liu, G., 2020. Defect-modified reduced graphitic carbon nitride (RCN) enhanced oxidation performance for photocatalytic degradation of diclofenac. *Chemosphere* 258, 127343. <https://doi.org/10.1016/j.chemosphere.2020.127343>.
- Karjadi, A.K., Karjadi Gunaeni, N., 2022. The effect of antiviral ribavirin, explant size, varieties on growth and development in potato meristematic. *IOP Conf. Ser.: Earth Environ. Sci.* 985, 012022 <https://doi.org/10.1088/1755-1315/985/1/012022>.
- Khan, N.E., Adewuyi, Y.G., 2010. Absorption and oxidation of nitric oxide (NO) by aqueous solutions of sodium persulfate in a bubble column reactor. *Ind. Eng. Chem. Res.* 49, 8749–8760. <https://doi.org/10.1021/ie100607u>.
- Koppenol, W.H., 2022. Ferryl for real. the Fenton reaction near neutral pH. *Dalton Trans.* 51, 17496–17502. <https://doi.org/10.1039/D2DT03168J>.
- Lian, W., Yi, X., Huang, K., Tang, T., Wang, R., Tao, X., Zheng, Z., Dang, Z., Yin, H., Lu, G., 2019. Degradation of tris(2-chloroethyl) phosphate (TCEP) in aqueous solution by using pyrite activating persulfate to produce radicals. *Ecotoxicol. Environ. Saf.* 174, 667–674. <https://doi.org/10.1016/j.ecoenv.2019.03.027>.
- Liu, Q., Feng, X., Chen, N., Shen, F., Zhang, H., Wang, S., Sheng, Z., Li, J., 2022. Occurrence and risk assessment of typical PPCPs and biodegradation pathway of ribavirin in wastewater treatment plants. *Environ. Sci. Ecotechnology* 11, 100184. <https://doi.org/10.1016/j.ese.2022.100184>.
- Liu, X., Hong, Y., Ding, S., Jin, W., Dong, S., Xiao, R., Chu, W., 2021. Transformation of antiviral ribavirin during ozone/PMS intensified disinfection amid COVID-19 pandemic. *Sci. Total Environ.* 790, 148030 <https://doi.org/10.1016/j.scitotenv.2021.148030>.
- Morales-Paredes, C.A., Rodríguez-Díaz, J.M., Boluda-Botella, N., 2022. Pharmaceutical compounds used in the COVID-19 pandemic: a review of their presence in water and treatment techniques for their elimination. *Sci. Total Environ.* 814, 152691 <https://doi.org/10.1016/j.scitotenv.2021.152691>.

- Rastogi, A., Al-Abed, S.R., Dionysiou, D.D., 2009. Sulfate radical-based ferrous-peroxymonosulfate oxidative system for PCBs degradation in aqueous and sediment systems. *Appl. Catal. B* 85, 171–179. <https://doi.org/10.1016/j.apcatb.2008.07.010>.
- Romero, A., Santos, A., Vicente, F., González, C., 2010. Diuron abatement using activated persulfate: effect of pH, Fe(II) and oxidant dosage. *Chem. Eng. J.* 162, 257–265. <https://doi.org/10.1016/j.cej.2010.05.044>.
- Shang, W., Dong, Z., Li, M., Song, X., Zhang, M., Jiang, C., Feiyun, S., 2019. Degradation of diatrizoate in water by Fe(II)-activated persulfate oxidation. *Chem. Eng. J.* 361, 1333–1344. <https://doi.org/10.1016/j.cej.2018.12.139>.
- Shi, X., Wang, Y., Jiao, J.J., Zhong, J., Wen, H., Dong, R., 2018. Assessing major factors affecting shallow groundwater geochemical evolution in a highly urbanized coastal area of Shenzhen City, China. *J. Geochem. Explor.* 184, 17–27. <https://doi.org/10.1016/j.gexplo.2017.10.003>.
- Su, C., Tang, C., Sun, Z., Hu, X., 2023. Mechanisms of interaction between metal-organic framework-based material and persulfate in degradation of organic contaminants (OCs): activation, reactive oxygen generation, conversion, and oxidation. *J. Environ. Manage.* 347, 119089 <https://doi.org/10.1016/j.jenvman.2023.119089>.
- Tarighi, P., Eftekhari, S., Chizari, M., Sabernavaei, M., Jafari, D., Mirzabeigi, P., 2021. A review of potential suggested drugs for coronavirus disease (COVID-19) treatment. *Eur. J. Pharmacol.* 895, 173890 <https://doi.org/10.1016/j.ejphar.2021.173890>.
- Tufail, A., Price, W.E., Mohseni, M., Pramanik, B.K., Hai, F.I., 2021. A critical review of advanced oxidation processes for emerging trace organic contaminant degradation: mechanisms, factors, degradation products, and effluent toxicity. *J. Water Process Eng.* 40, 101778 <https://doi.org/10.1016/j.jwpe.2020.101778>.
- Wang, Z., Jiang, J., Pang, S., Zhou, Y., Guan, C., Gao, Y., Li, J., Yang, Y., Qiu, W., Jiang, C., 2018. Is sulfate radical really generated from peroxydisulfate activated by Iron(II) for environmental decontamination? *Environ. Sci. Technol.* 52, 11276–11284. <https://doi.org/10.1021/acs.est.8b02266>.
- Wang, Z., Du, C., Lei, S., Ding, D., Chen, R., Yang, S., Cai, T., 2021. Modulation of carbon induced persulfate activation by nitrogen dopants: recent advances and perspectives. *J. Mater. Chem. A* 9, 25796–25826. <https://doi.org/10.1039/D1TA08335J>.
- Wang, J., Wang, S., 2018. Activation of persulfate (PS) and peroxymonosulfate (PMS) and application for the degradation of emerging contaminants. *Chem. Eng. J.* 334, 1502–1517. <https://doi.org/10.1016/j.cej.2017.11.059>.
- Wu, X., Zhang, J., Hu, S., Zhang, G., Lan, H., Peng, J., Liu, H., 2022. Evaluation of degradation performance toward antiviral drug ribavirin using advanced oxidation process and its relations to ecotoxicity evolution. *Sci. Total Environ.* 850, 157851 <https://doi.org/10.1016/j.scitotenv.2022.157851>.
- Xu, X.-R., Li, X.-Z., 2010. Degradation of azo dye Orange G in aqueous solutions by persulfate with ferrous ion. *Sep. Purif. Technol.* 72, 105–111. <https://doi.org/10.1016/j.seppur.2010.01.012>.
- Yan, Y., Wei, Z., Duan, X., Long, M., Spinney, R., Dionysiou, D.D., Xiao, R., Alvarez, P.J. J., 2023. Merits and limitations of radical vs. nonradical pathways in persulfate-based advanced oxidation processes. *Environ. Sci. Technol.* 57, 12153–12179. <https://doi.org/10.1021/acs.est.3c05153>.
- Yang, Y., Pignatello, J.J., Ma, J., Mitch, W.A., 2014. Comparison of halide impacts on the efficiency of contaminant degradation by sulfate and hydroxyl radical-based advanced oxidation processes (AOPs). *Environ. Sci. Technol.* 48, 2344–2351. <https://doi.org/10.1021/es404118q>.
- Ye, D., Bao, Z., Yu, Y., Han, Z., Yu, Y., Xu, Z., Ma, W., Yuan, Y., Zhang, L., Xu, Y., Ma, T., Liu, S., Gao, X., Yan, G., Huang, Q., Wang, X., Hua, B., Yang, F., Li, Y., Cai, B., 2020. Inhibition of cardiomyocyte differentiation of human induced pluripotent stem cells by ribavirin: implication for its cardiac developmental toxicity. *Toxicology* 435, 152422. <https://doi.org/10.1016/j.tox.2020.152422>.
- Zeng, G., Yang, R., Fu, X., Zhou, Z., Xu, Z., Zhou, Z., Qiu, Z., Sui, Q., Lyu, S., 2021. Naphthalene degradation in aqueous solution by Fe(II) activated persulfate coupled with citric acid. *Sep. Purif. Technol.* 264, 118441 <https://doi.org/10.1016/j.seppur.2021.118441>.
- Zhang, K., Parker, K.M., 2018. Halogen radical oxidants in natural and engineered aquatic systems. *Environ. Sci. Technol.* 52, 9579–9594. <https://doi.org/10.1021/acs.est.8b02219>.
- Zhang, K., Zhou, X., Zhang, T., Yu, L., Qian, Z., Liao, W., Li, C., 2018. Degradation of the earthy and musty odorant 2,4,6-trichloroanisole by persulfate activated with iron of different valences. *Environ. Sci. Pollut. Res.* 25, 3435–3445. <https://doi.org/10.1007/s11356-017-0452-x>.
- Zhou, X., Yin, R., Kang, J., Li, Z., Pan, Y., Bai, J., Li, A.J., Qiu, R., 2023. Atomic cation-vacancy modulated peroxymonosulfate nonradical oxidation of sulfamethoxazole via high-valent iron-oxo species. *Appl. Catal. B* 330, 122640. <https://doi.org/10.1016/j.apcatb.2023.122640>.